View metadata, citation and similar papers at core.ac.uk

brought to you by CORE

provided by Elsevier - Publisher Connector

NEOPLASIA
www.neoplasia.com

Volume 10 Number 10 October 2008 pp. 1028–1040 1028

Noninvasive Monitoring of Breast Cancer during Neoadjuvant Chemotherapy Using Optical Tomography with Ultrasound Localization[1,2]

Quing Zhu*, Susan Tannenbaum†, Poornima Hegde‡, Mark Kane§, Chen Xu* and Scott H. Kurtzman†,¶

*Bioengineering Program, Electrical and Computer Engineering Department, University of Connecticut, 371 Fairfield Rd, U2157, Storrs, CT 06269, USA; †Neag Cancer Center, University of Connecticut Health Center, 263 Farmington Avenue, Farmington, CT 06030, USA; ‡Pathology Department, University of Connecticut Health Center, 263 Farmington Avenue, Farmington, CT 06030, USA; §Radiology Department, University of Connecticut Health Center, 263 Farmington Avenue, Farmington, CT 06030, USA; ¶Department of Surgery, University of Connecticut Health Center, Waterbury Hospital Medical Center, 263 Farmington Avenue, Farmington, CT 06030, USA

Abstract

The purposes of this study were 1) to investigate the feasibility of using optical tomography in the near-infrared (NIR) spectrum combined with ultrasound (US) localization (NIR/US) in monitoring tumor vascular changes and assessing tumor pathological response during chemotherapy and 2) to compare the accuracy of NIR/US with magnetic resonance imaging (MRI) in predicting residual cancer after neoadjuvant chemotherapy. Eleven female patients were studied during treatments with a combined imager consisting of a commercially available US system coupled to an NIR imager. Contrast-enhanced MRI was performed before treatment and surgery. Tumor vascular content was assessed based on total hemoglobin concentration and volume obtained from NIR data. A percentage blood volume index (%BVI) was calculated as the percentage ratio of the product of total hemoglobin concentration and volume normalized to pretreatment values. At treatment completion, pathologic assessment revealed three response groups: complete or near-complete responders (A), partial responders (B), and nonresponders (C). The mean %BVIs of groups A, B, and C at the treatment completion were 29.1 ± 6.9%, 46.3 ± 3.7%, and 86.8 ± 30.1%, respectively (differences statistically significant, $P < .04$). At the end of cycle 2, the %BVI of group A was noticeably lower than that of the partial ($P = .091$) and nonresponder groups ($P = .075$). Both NIR/US and MRI were equally effective in distinguishing different response groups in this pilot study. Our initial findings indicate that NIR/US using %BVI can be used during chemotherapy to repeatedly monitor tumor vascular changes. NIR/US also may evaluate pathologic response during treatment allowing for tailoring therapies to response.

Neoplasia (2008) 10, 1028–1040

Introduction

Neoadjuvant chemotherapy is being used more frequently for patients with stage II or stage III breast cancer [1]. When used before surgery, it often allows for breast conservation by reducing tumor size [2]. An additional benefit of neoadjuvant chemotherapy is the opportunity to assess the chemoresponsiveness of the tumor *in vivo*. Moreover, important prognostic information is obtained; when a pathologically complete response is achieved, patients have

Address all correspondence to: Quing Zhu, Professor of Bioengineering Program, Electrical and Computer Engineering Department, University of Connecticut, Storrs, CT. E-mail: zhu@engr.uconn.edu

[1]This work is supported by the National Institutes of Health (R01EB002136) and The Patrick and Catherine Weldon Donaghue Medical Research Foundation.
[2]This work was presented in part at the 30th Annual San Antonio Breast Cancer Symposium, Dec 13 to 16, 2007 (General Session 4 Abstract No. 45).
Received 16 May 2008; Revised 20 June 2008; Accepted 23 June 2008

Copyright © 2008 Neoplasia Press, Inc. All rights reserved 1522-8002/08/$25.00
DOI 10.1593/neo.08602

increased disease-free and overall survival [3,4]. Because there are many new agents available for the treatment of breast cancer, it is important to monitor tumor response so the best therapy can be used in each setting [5].

Conventional methods to monitor response to neoadjuvant chemotherapy include physical examination, ultrasonography (US), and mammography. However, they have been shown to be only moderately useful for predicting residual pathologic tumor size after neoadjuvant chemotherapy [1,6]. A study comparing these three methods in 189 patients treated with neoadjuvant chemotherapy found all three had correlation coefficients of 0.41 to 0.42 with residual tumor [6]. More recently, magnetic resonance imaging (MRI) has been increasingly used to evaluate neoadjuvant chemotherapy of locally advanced breast cancers [1,7]. Several studies have assessed the use of MRI performed early in neoadjuvant treatment for predicting subsequent clinical or pathologic tumor response [8–10]. Other studies have evaluated the residual disease after the neoadjuvant treatment before surgery and demonstrated that lesion size measured by MRI after treatment correlates well with residual tumor evaluated by pathology [11,12]. However, because of the potential for false-negative MRI determinations after neoadjuvant treatment, a phenomenon that has been attributed to diminished contrast enhancement due to the antiangiogenetic effect of treatment, surgery remains an important procedure for all patients including those with no evidence of residual disease on postchemotherapy MRI [7]. Positron emission tomography (PET) is a promising technique both for predicting neoadjuvant treatment at early stage [13] and for assessment of residual disease [14]. There are many ongoing studies to assess the predictive value of PET in the neoadjuvant setting [1].

Near-infrared (NIR) light between the wavelengths of 650 and 900 nm propagates deeply through tissues. Diffuse optical tomography using NIR light provides a unique approach for functional and molecular-based diagnostic imaging of the breast and for monitoring the chemotherapeutic response of breast cancers [15–34]. The primary limitation of diffuse optical tomography is related to the fact that multiple scattering dominates NIR light propagation in tissues, making three-dimensional localization of lesions and accurate quantification of lesion optical properties difficult. Recently, optical tomography guided by co-registered MRI, X-ray, and US has demonstrated a great potential to overcome lesion location uncertainty and to improve light quantification accuracy [26,28,29,31–33]. We have introduced the US-guided optical tomography technique (NIR/US), which uses co-registered US to localize breast lesions and optical tomography to image tumor total hemoglobin (tHb) distribution, which is directly related to blood vessel density in tumors. We have shown that, on average, the tHb concentration of early-stage malignant cancers is twice that found in benign breast lesions [31,32]. We have also observed heterogeneous tHb distributions from a small number of patients who have advanced cancers and showed that the distorted distributions correlate with histologic microvessel density (MVD) counts [33]. In this article, we report our initial experience with serial observations using NIR/US in a group of patients with large palpable breast cancers treated with neoadjuvant chemotherapy. A novel volumetric measurement of tHb has been introduced to quantitatively evaluate the treatment response. The objectives of the study using NIR/US were to assess how tumor vasculature reacts to neoadjuvant treatment and to determine how well the vascular response correlates with the tumor pathologic response. Another study objective is to compare the vascular response measured by NIR/US with that measured by contrast-enhanced MRI.

Materials and Methods

Subjects

The study cohort included 16 consecutive patients who were referred for neoadjuvant chemotherapy and agreed to participate in our study. These patients were treated at the Neag Cancer Center of the University of Connecticut from March 2004 to June 2007. The study protocol was approved by the university institutional review board, and signed informed consent was obtained from all patients. Eleven of 16 patients completed the study and were repeatedly imaged by NIR/US before initiation of chemotherapy, at intervals of two, four, and six cycles during chemotherapy, and before definitive surgery. Four patients did not complete the study either due to a change in their treatment plan or due to unwillingness to continue to participate. One patient was studied only once before her definitive surgery. Table 1 (columns 1 to 7) presents the clinical characteristics of the final study group. This includes assessment of tumor size by clinical examination at the initial presentation and at the completion of neoadjuvant chemotherapy. The initial tumor depth estimated by palpation and US is also given in Table 1 (column 3). The histologic type in 10 of these patients was invasive ductal carcinoma; one patient had a

Table 1. Physical Exam Results (Columns 2 to 3), Tumor Characteristics (Columns 4 to 7) and Surgical Pathology (Columns 8 to 9).

Patient No./Age	Size (cm)/PE Pre/Post	Depth (cm)	Type	Nottingham Score (Out of 9)/Grade	ER/PR	HER2 Pre	Residual Tumor	Response (%)/Category (A-D)
1/67	4/0	1.5	ID	8/III	–/–	–	Microscopic foci	>99/A
2/57	4/0	2.5	ID	9/III	+/+	–	Microscopic foci	>99/A
3/66	4/0	1.5	ID	8/III	–/–	+	None	100/A
4/54	6/0	2.0	ID	9/III	+/–	–	2.4 cm	70/B
5/39	2/0	2.0	ID	9/III	–/–	–	1.5 cm	80/B
6/55	5/0	2.0	ID	9/III	–/–	+	1.5 cm	70/B
7/53	NE	~2.0	ID	8/III	–/–	–	5.1-cm mass with scar, calcification, necrosis Foci of residual invasive carcinomas, larger foci, 0.5 cm	75/B
8/42	4/1	1.0	ID and L, post-IL	6/II	+/+	+	1.2 cm	30/C
9/47	4/5	2.0	ID	5/II	+/+	–	2.0 cm	5/C
10/49	3/0	1.5	ID	6/II	+/+	–	1.4 cm	5/C
11/49	4/0	1.0	ID	4/I	+/+	–	3.3 cm	5/C

ID indicates infiltrating ductal; *IL*, infiltrating lobular; *PE*, physical examination; *NE*, scar size indeterminate.

mixed ductal and lobular carcinoma. Invasive carcinoma within the pretreatment core biopsies was graded by using the Nottingham histologic score. Estrogen receptor, progesterone receptor, and Neu-Her2/CerbB-2 immunohistochemistry was performed on formalin-fixed, paraffin-embedded tissue using the DakoEnvision+ (Dako Denmark A/S, Glostrup, Denmark) detection system. The estrogen and progesterone receptors were scored by the modified San Antonio Scoring system. Test for Her-2/neu gene amplification was performed by fluorescence *in situ* hybridization technique with the PathVision HER-2 DNA probe kit from Abbott Molecular Inc. (Des Plaines, IL). The results were reported as the ratio of HER-2/neu to CEP 17. A ratio greater than 2.0 is considered amplification of this gene.

Nine patients were treated with anthracycline and taxane. Of the remaining three patients, two were treated as part of a protocol containing capecitabine and docetaxel (with one of the two receiving herceptin). The remaining HER2-positive patient was treated with carboplatin, docetaxel, and herceptin. All 11 patients received the first cycle of neoadjuvant chemotherapy an average of 5 days (range, 0 to 21 days) after the initial NIR/US study. The average interval between the last treatment and posttreatment NIR/US was 14 days (range, 2 to 33 days). The average interval between posttreatment NIR/US and surgery was 17 days (range, 1 to 46 days). Eight patients had pretreatment MRI an average of 2 days (range, 5 to 40 days) before the treatment and two patients who refused MRI because of claustrophobia had pretreatment X-ray computed tomography (CT)/PET before the treatment. One patient had pretreatment MRI 12 days after the first treatment due to scheduling problems and her MRI data were not used for evaluation of imaging response. The average interval between the last treatment and posttreatment MRI was 14 days (range, 7 to 26 days). The average interval between posttreatment MRI and surgery was 22 days (range, 7 to 48 days). Surgery was performed after eight (n = 6), six (n = 1), and four cycles of treatment (n = 4). After completion of primary chemotherapy, eight patients underwent lumpectomy and three underwent mastectomy.

NIR Imaging System, Measurements, and Imaging Algorithm

A hand-held hybrid probe was used, consisting of the commercially available US transducer L12 for a Phillips IU22 system (Philips Electronics North America Corporation, New York, NY) located in the middle and NIR source-detector light guides (optical fibers) distributed at the periphery (Figure 1). The technical aspects of the NIR imager developed by our group have been described in detail previously [35,36]. Briefly, our first prototype imager consisted of 12 pairs of 780- and 830-nm laser diodes and the second prototype consisted of one set of 690-, 780-, and 830-nm laser diodes and 3 × 1 and 1 × 9 optical switches that delivered the light to nine source locations. On the receiving side, 8 (first prototype) or 10 (second prototype), 3-mm-diameter light guides were used to couple reflected light to photomultiplier tubes (R928; Hamamatsu, Shizuoka, Japan). The total number of source and detector pairs of both systems was comparable and consequently achieved similar imaging quality. The addition of the 690-nm wavelength in the second prototype was not used in the tHb computation reported in the article but was used in the oxygen saturation estimation (see the Discussion). The light was delivered to each source position sequentially and reflected light was detected in parallel from all photomultiplier tube detectors. The entire acquisition from all source detector pairs took about 3 to 4 seconds. For each patient, co-registered US images and optical measurements were acquired simultaneously at multiple locations including the lesion region and a normal region of the same quadrant as the lesion in the contralateral breast, which was chosen as the reference site. The difference between measurements obtained from the lesion site and the reference site was the scattered field and was used for optical imaging reconstruction. This is a standard perturbation approach initially introduced in Ref. 37. Presumably, any changes related to normal breast tissue response to chemotherapy at each assessment point was subtracted out in this approach.

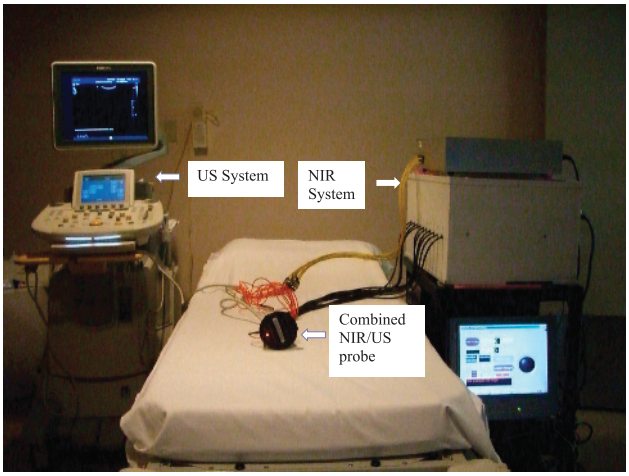

Figure 1. Combined US and NIR systems and a hand-held probe with a centrally located US linear array and NIR source-detector fibers distributed at the periphery of the probe.

Details of the dual-zone mesh optical-imaging reconstruction algorithm with experimental validation have been described elsewhere [30,36]. Briefly, the NIR reconstruction takes advantages of US localization of lesions and segments the imaging volume into a finer grid in lesion region L and a coarser grid in non–lesion background region B. In all images, a 0.5 cm × 0.5 cm × 0.5 cm imaging grid was used for the lesion and a 1.5 cm × 1.5 cm × 1 cm grid was used for the background region. The total imaging volume is chosen to be 9 × 9 × 4 (cm^3). A modified Born approximation is used to relate the scattered field U_{sd} measured at each source (s) and detector pair (d) to total absorption variations at wavelength λ in each volume element of two regions within the sample. The matrix form of image reconstruction is given by

$$[U_{sd}]_{M\times 1} = [W_{\mathrm{L}}, W_{\mathrm{B}}]_{M\times N}[M_{\mathrm{L}}, M_{\mathrm{B}}]^{T}{}_{N\times 1}, \qquad (1)$$

where W_{L} and W_{B} are weight matrices for lesion and background regions, respectively, and are calculated from the background absorption and reduced scattering measurements acquired at the normal contralateral breast. M_{L} and M_{B} are the to-be-determined total absorption distribution changes of lesion and background regions, respectively. The absorption distribution at each wavelength is obtained by dividing M_{L} and M_{B} with different voxel sizes in lesion and background tissue regions. With this dual-mesh scheme, the inversion is well conditioned and the image reconstruction converges in a few iterations.

Optical absorption distribution at each wavelength was reconstructed and tHb distribution was computed from absorption maps at 780 and 830 nm. Maximum and average tumor tHb concentration (maxtHb and avetHb) were measured and the average was computed within the volumetric zone exceeding 50% of the maximum value. The standard full width at half-maximum (FWHM) tHb image was

used to measure the tumor diameter in three dimensions noted as D_X, D_Y, and D_Z. The blood volume index (BVI) is defined as the product of maximum diameters D_X, D_Y, and D_Z in two spatial dimensions and in depth, and the avetHb of the tumor, i.e., BVI = $D_X \times D_Y \times D_Z \times$ avetHb. The BVI obtained before treatment is taken as the baseline for each patient and the percentage blood volume index (%BVI) normalized to the baseline is used to quantitatively evaluate the tumor blood volume changes during chemotherapy. %BVI normalizes each individual patient's response to pretreatment and facilitates the assessment of changes during treatment.

US/MRI Assessment of Tumor Response

In all patients, US images were acquired and the largest tumor sizes in spatial dimensions and in depth were measured. Breast MRI was performed using a Siemens unit with a field strength of 1.5 T. Breast MRI images were acquired before and after 20-ml gadolinium injection. The precontrast sequence includes inversion recovery as well as T1 and T2 fat saturation images followed by a dynamic sequence of T1-weighted images. This sequence entails one noncontrast set immediately followed by five consecutive postcontrast sets. Subtraction of each of the five postcontrast sets from the precontrast set is used to evaluate lesions. The size of the tumor is measured from MRI in craniocaudal (CC), transverse (T), and anterior-posterior (AP) dimensions. One patient (patient 8) had two lesions. As recommended in Ref. 37, the sum of the two volumes is used as the total volume for computing the fractional change. One radiologist (M.K.) performed these measurements while being blinded to the optical imaging results.

Image response as measured by US and MRI was determined according to published criteria involving changes in tumor volume after chemotherapy [38]. The percentage reduction in volumetric measurements of US and MRI is shown in Table 2. Complete response indicated disappearance of the primary tumor, partial response indicated a volume reduction of at least 65%, and progressive disease

Table 2. Imaging Findings.

Patient (Response Category)	MRI CC × T × AP (cm)	% Reduction	US (cm)	% Reduction	Hb Level, Max tHb/ Ave tHb (μM/l)	Pattern FWHM (cm^3)	%BVI	% Reduction
1 (A)	CT		4.4 × 4.4 × 2.7	100	83.8/54.3	6.2 × 5.0 × 2.0	100	
	3.2T × 3.2AP	N/A	1.5 × 1.5 × 1.2		83.3/54.6	5.0 × 5.4 × 1.5	65.7	
			No residual tumor mass		78.0/54.4	3.4 × 3.9 × 1.5	32.1	67.9
2 (A)	3.5 × 4 × 4		2.8 × 2.8 × 1.8	100	57.6/40.0	4.1 × 4.5 × 2.0	100	
	No residual tumor mass	100	1.3 × 1.3 × 0.9		47.7/32.2	3.0 × 4.5 × 2.0	58.9	
			0.6 × 0.6 × 0.4		34.1/23.9	3.5 × 4.8 × 1.5	40.8	
			No residual tumor mass		55.4/38.2	2.5 × 3.5 × 1.5	34.0	66.0
3 (A)	1.8 × 2.0 × 3.7		2.3 × 2.5 × 1.3	100	115.5/73.9	4.1 × 3.5 × 2.0	100	
	No residual tumor mass	100	2.5 × 2.5 × 0.3		72.5/52.1	4.0 × 5.5 × 1.0	54.0	
			No residual tumor mass		53.0/36.6	3.0 × 4.1 × 1.0	21.2	78.8
Ave. of group A		100 (±0)		100 (±0)			29.1 (±6.9)	70.9 (±6.9)
4 (B)	CT		2.7 × 2.7 × 2.5		110.9/69.0	5.5 × 6.7 × 2	100	
	5.3T × 4.3AP	N/A	1.9 × 1.9 × 2.0		85.6/56.3	4.0 × 4.8 × 2	42.5	
			2.1 × 2.1 × 1.4	89	85.0/54.6	5.3 × 4.3 × 2	48.9	
			1.5 × 1.5 × 0.9		72.6/46.5	4.8 × 5.4 × 2	47.4	52.6
5 (B)			3.3 × 3.3 × 2.2		109.1/72.4	3.4 × 3.4 × 2.0	100	
	3.3 × 4.0 × 5.4		1.9 × 1.9 × 1.2		89.3/60.9	4.7 × 4.0 × 1.5	102.6	
	1.3 × 1.2 × 1.0	98	1.1 × 1.1 × 0.8	94	57.0/37.0	3.5 × 4.2 × 1.5	48.7	
			1.4 × 1.1 × 0.9		56.9/37.9	3.5 × 4.2 × 1.5	49.9	50.1
6 (B)			3.1 × 3.1 × 2.0		74.7/48.3	4.9 × 3.9 × 2.5	100	
	2.7 × 2.1 × 4.4		2.6 × 2.6 × 1.6		72.7/48.3	4.0 × 5.9 × 2.0	98.8	
	0.8 × 1.1 × 1.0	96	1.3 × 1.3 × 0.9	98	49.0/33.0	4.5 × 5.4 × 2.0	69.5	
			0.8 × 0.8 × 0.6		61.5/42.0	2.9 × 4.4 × 2.0	46.5	53.5
7 (B)			5.2 × 5.2 × 3.0		131.7/86.2	5.8 × 7 × 2.5	100	
	4.4 × 3.7 × 2.8		5.2 × 5.2 × 3.0		134.7/89.7	6 × 5.9 × 2.5	90.7	
	1.2 × 1.4 × 1.2	97	4.3 × 4.3 × 2.5	40	136.6/90.8	4.5 × 4.6 × 2.5	53.7	
			4.4 × 4.4 × 2.5		113.8/72.8	4.5 × 4.4 × 2.5	41.2	58.8
Ave. of group B		97 (±1)		80.3 (±27.1)			46.3 (±3.7)	53.8 (±3.7)
8 (C)	#1: 2.7 × 2.1 × 2.3		3.5 × 3.5 × 1.5		93.3/59.3	4.0 × 7.0 × 1.5	100	
	#1: 1.9 × 1.7 × 1.5	63	3.3 × 3.3 × 1.3		106.4/70.0	3.3 × 6.9 × 1.5	96.0	
	#2: 1.4 × 1.5 × 1.2	Sum	1.8 × 1.8 × 1.0	83	99.4/67.8	3.2 × 5.3 × 1.5	69.3	30.7
	#2: 0.8 × 0.6 × 0.8	85, 66						
9 (C)			3.8 × 4.0 × 2.5		152.0/98.0	4.5 × 4.5 × 2.5	100	
	2.8 × 2.3 × 2.8		2.9 × 2.9 × 1.8		143.3/96.4	3.5 × 4.0 × 2.5	68.0	
	2.0 × 1.9 × 2.1	56	2.7 × 2.1 × 2.0	70	112.8/76.0	3.5 × 4.0 × 2.5	53.6	46.4
10 (C)			2.2 × 2.5 × 1.4		72.0/49.0	3.5 × 3.6 × 2	100	
	N/A		2.0 × 2.0 × 1.3		72.9/49.4	3.8 × 3.6 × 2	109.5	
			2.0 × 2.0 × 1.3	32	67.9/44.1	4.5 × 3.6 × 2	115.7	−15.7
11 (C)			3.2 × 3.2 × 2.0		131.1/86.8	4.5 × 4 × 2	100	
	3.8 × 2.8 × 2.3	16	2.7 × 2.7 × 1.7		125.1/81.2	5.0 × 4.8 × 2	124.7	
	2.3 × 3.0 × 2.6		1.9 × 1.9 × 1.7		118.4/77.3	4.0 × 4.4 × 2	87.1	
			1.3 × 1.3 × 1.5	88	123.0/80.0	4.8 × 3.5 × 2	86.0	
			1.3 × 1.3 × 1.5		123.7/84.7	5.0 × 4.0 × 2	108.4	−8.4
Ave. of group C		46 (±26.5)		68.3 (±25.3)			86.8 (±30.1)	13.3 (±30.1)

N/A indicates not available.

indicated a volume increase of at least 73%. Stable disease corresponded to all other cases that were not in the other three categories.

Pathological Assessment of Tumor Response

In all study patients, the core and definitive surgical specimens were previously signed out by attending pathologists as and when the specimens were received in the department of pathology. The information about any residual tumor with gross and/microscopic measurements as well as histologic evidence of necrosis, fibrosis, and calcification, if any, was also previously documented within the pathology reports. Two authors (P.H. and S.T.) compiled the tumor responses by using the grading scale established by Sataloff et al. [39]. The grading of pathologic response reproduced within the breast specimens is as follows: total or near-total therapeutic effect (grade A), more than 50% therapeutic effect but less than total or near-total effect (grade B), less than 50% therapeutic effect but visible effect (grade C), or no therapeutic effect (grade D). Therapeutic effect is defined by microscopic changes such as fibrosis, necrosis, myxoid change, hemosiderin deposition, calcifications, or foamy macrophages with or without inflammatory infiltration. A quantitative assessment of these changes within the definitive surgical specimens in comparison to the needle core biopsies was expressed as percent reduction of tumor (Table 1, column 9). These two authors were blinded to the optical imaging results.

Histological Determination of MVD

MVD was determined within final definitive surgical specimens of the primary tumor. The specimens were fixed as described earlier. Paraffin sections (5 μm) were dewaxed in xylene and hydrated through serial alcohol. The sections were stained with hematoxylin and eosin for pathologic evaluation. One to two blocks of the tumor were selected for CD31 immunostain (clone JC70A, Dako autostainer). Block selection was preferably from the anterior and posterior portions of the tumor to correspond to the anterior and posterior planes of tHb concentrations measured from NIR images. Immunostained slides were evaluated for vessel density using an ocular grid to count the vessels within 10 consecutive fields of 200× magnification. Vessel counts were performed within the areas of invasive carcinoma starting from the highest vascular spots within the sample [40]. In patients who demonstrated total or near-total therapeutic response, the location of the preexisting tumor was determined by the clip. Histologically, this area was marked by fibrosis with focal chronic inflammation. An average of two vessel-count readings performed within a 5-mm radius around the fibrosis was calculated and represented the MVD after neoadjuvant therapy. One pathologist (P.H.) performed these studies while being blinded to the optical imaging results.

Statistical Analysis

A two-sample t test with unpooled variance estimate was used to calculate statistical significance between groups. NIR %BVI data and US and MRI volumetric reduction data were tested for normality first using Bera-Jarque test at the significance level of $\alpha = 0.05$. Each data set is from a normal distribution without outliers.

Results

Patient and Tumor Characteristics

The clinical characteristics of the patients and their tumors are presented in Table 1 (columns 1 to 7). None of the patients had bilateral disease. Six of seven patients with high-grade tumors were postmenopausal (average age, 59 years), whereas patients with all low- to intermediate-grade tumors were premenopausal (average age, 47 years). The average size of the high-grade tumors was 4.1 cm and that of the lower grade tumors 3.8 cm. One of 11 patients had an indeterminate-sized tumor by examination, as her cancer recurred in the scar of a previously irradiated breast. She went on for mastectomy with clear margins as is the standard of care in that setting. Of the remaining 10 patients, eight had lumpectomies and two underwent mastectomies. Both mastectomies were performed in patients with small breast size and lower grade cancers. Interestingly, both of these patients had complete or near-complete clinical responses by physical examination. Nine of 11 patients had clinical complete responses and one of 11 had stable disease.

Correlation of NIR/US with Pathological Response

Residual tumor evaluated from surgical pathology and the tumor response category are given in Table 1 (columns 8 and 9). Three of 11 patients, all with high-grade tumors, had a complete or near-complete pathologic response (group A). The tumor bed of the near-complete responders contained a few viable tumor cells remaining in a sea of stroma. Four of the remaining patients, again all grade III, had a significant partial response with a 70% reduction in tumor burden (group B). The four remaining patients with lower grade tumors had a minimal to absent response (group C). These nonresponders were all estrogen and progesterone receptor positive and had HER2-negative tumors except one case with two tumor types.

Calculated %BVI at treatment completion accurately reflects the three groups seen pathologically (Figure 2, red bar) in this pilot study. The mean %BVIs and standard deviations were 29.1 ± 6.9%, 46.3 ± 3.7%, and 86.8 ± 30.1% for groups A, B, and C, respectively. The %BVI in group A is significantly lower than in B ($P < .02$) and C ($P < .02$), whereas the %BVI in group B is significantly lower than in C ($P < .04$). The mean %BVI and standard deviation of the responder group (A + B) is 38.9 ± 10.3%, which is considerably lower than that of nonresponders in group C ($P < .04$).

To assess the potential of NIR/US in predicting early response, the %BVIs at the end of cycle 2 were reviewed (Figure 2, blue bar). The

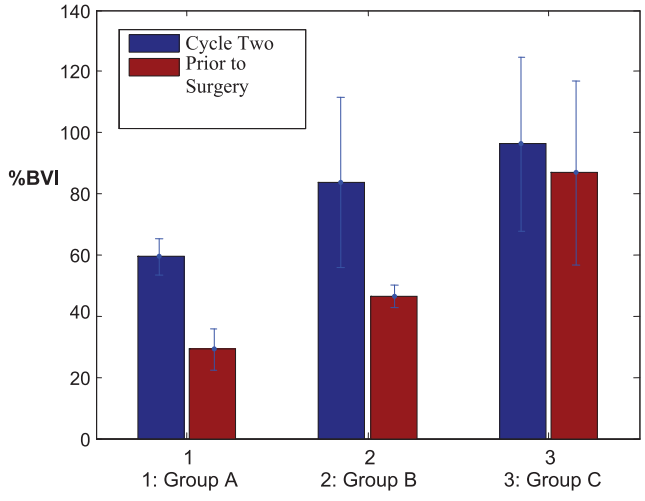

Figure 2. %BVI obtained from complete/near-complete responder group A, partial responder group B, and nonresponder group C at the end of cycle 2 (blue bars) and before surgery (red bars).

mean %BVIs and the standard deviations were 59.5 ± 5.9%, 83.7 ± 27.9, and 96.2 ± 28.4% for groups A, B, and C, respectively. The %BVI of group A is noticeably lower than those of the partial (P = .091) and nonresponder groups (P = .075); however, the statistical significance is moderate. This is mainly due to the larger standard deviations of groups B and C. There is no noticeable difference between B and C (P = .294). The %BVIs from responders (A + B) and nonresponders obtained at the end of each treatment course were also reviewed. The mean %BVI of the responder group (73.3 ± 23.8%) is lower than that of the nonresponder group (96.2 ± 28.4%) at the end of cycle 2; however, the statistical difference is weak (P = .15). The mean %BVI of the responder group is significantly lower than that of the nonresponder group at the end of treatment (P = .023).

MRI/US and NIR imaging data are given in Table 2. Three types of vascular response patterns from the chemoresponsive group (A + B) were observed in NIR images. The first pattern was characterized by a significant reduction in size measured by FWHM from the tHb image, but not much reduction in tHb level or its functional activity (Figure 3). The second pattern was characterized by a reduction in both tHb level and size (Figure 4). Five patients in groups A and B belong to this category. The third pattern was characterized as significant reduction in tHb level but only a small change in size. In addition to the complex tHb patterns discussed above, two lobulated carcinomas (patients 1 and 4) showed highly heterogeneous tHb distributions before treatment; the distribution was more uniform after two cycles of treatment. Two of four nonresponding patients showed no observable reduction or increase in %BVI (Figure 5). In these two patients, both tHb level and tumor size demonstrated either no change or an increase throughout the treatment period.

US and MRI Imaging Results

The percentage reduction in volumetric measurements of US is shown in Table 2. The averages and standard deviations of groups A, B, and C are 100 ± 0%, 80.3 ± 27.1%, and 68.3 ± 25.3%, respectively. No statistical significance was found between groups A and B and between groups B and C at the significance level of .05. No statistical significance was found between the responder and nonresponder groups at the same significance level. The difference between groups A and C is significant (P < .05). If US were used for predicting the response, three patients in group C would be misclassified into B, whereas one patient in group B would be in C.

The average volumetric reduction in MRI of groups A, B, and C are 100 ± 0% (n = 2), 97.0 ± 1.0% (n = 3), and 46 ± 26.5% (n = 3). Statistical significance was found between groups A and B (P < .02), A and C (P < .04), and B and C (P < .04). Statistical significance (P < .04) was found between responders (98.2 ± 1.8%, n = 5) and nonresponders (n = 3). If MRI were used for predicting response, one patient in group C (patient 8) could be misclassified into group B.

Linear regression analysis between the volumetric reduction in MRI and %BVI in NIR obtained a correlation coefficient of 0.914, which is statistically significant (P < .002), whereas the same analysis between volumetric reduction in US and %BVI obtained a correlation coefficient of 0.510, which showed no statistical significance (P = .109).

MVD and Correlation with tHb Measurements

Figure 6 shows the MVD counts obtained from the anterior and posterior portions of invasive carcinoma within the surgically resected breast specimens versus measured maximum tHb at the corresponding planes in the tHb images. Linear regression analysis obtained 0.4577 correlation coefficient, which is moderately significant (P = .056). Note that for patients with residual tumors, two blocks from the anterior and posterior portions of the tumor, which corresponded to the anterior and posterior planes of tHb concentrations, measured from NIR images were selected for MVD counts. One data point obtained from a partial responder (surgery was performed at another hospital) was an outlier and was removed to obtain the linear regression curve. The mean MVDs and standard deviations of responders and nonresponders were 77.6 ± 23.15 and 89.8 ± 18.96, respectively. No statistical significance was found between these two groups on MVD at the significance level of .05.

Discussion

The objective of this study was to assess how tumor vasculature reacts to treatment and how these changes are measured with noninvasive NIR/US technology. Total hemoglobin concentration measured by this technology directly correlates to MVD, as shown in this study (Figure 6) and in an earlier study [33]. However, we found in this study that there was no statistical difference between responders and nonresponders in MVD. Makris et al. [41] reported lower tumor microvessel counts in patients with breast cancer treated with chemoendocrine therapy compared with untreated patients. However, the authors reported no statistical differences in MVD between responders and nonresponders. %BVI is a novel way of measuring blood vessel density, taking into consideration tHb concentration and vessel mass by volumetric measurements. Recently, optical tomography has been explored by several research groups for its potential role in monitoring response to chemotherapy [18,27,33,41]. Case reports from these groups are consistent with our results revealing that most responders demonstrate a reduction in tHb level during chemotherapy. However, we found in this pilot study that tHb or MVD does not correlate to pathologic response if volumetric measures are not included.

All responding patients (A + B) showed a reduction in %BVI. The reduction is never 100% but was as large as 79% in our one complete responder. It is possible that the rapidly proliferating components of the vasculature and more immature components regress, leaving a better differentiated, more established vasculature that is slow to regress [42]. There was no single pattern of response: some had volume reductions without change in tHb; others had tHb reduction with no change in volume; others had a combination of volume and tHb reduction. This heterogeneity of response may be explained in part by the differential chemosensitivity of the vasculature or the tumor and host.

Gene expression analysis has identified three major breast cancer subtypes [43] that have different prognoses [44]. However, a recent study has shown that patients who had pathologically complete response to chemotherapy had a good prognosis regardless of subtype [45]. Thus the correlation between vascular response, as measured by %BVI, and complete or near-complete pathologic response is very important clinically. If one can accurately monitor response repeatedly and as easily as performing a US exam, systemic therapy can be altered so the most efficacious drugs could be used. Ideally, chemotherapy should be monitored at earlier cycles as this could facilitate modification of the regimen to enable the lesion to be maximally treated and for the treatment response to be observed [8–10,13,34]. In a recent

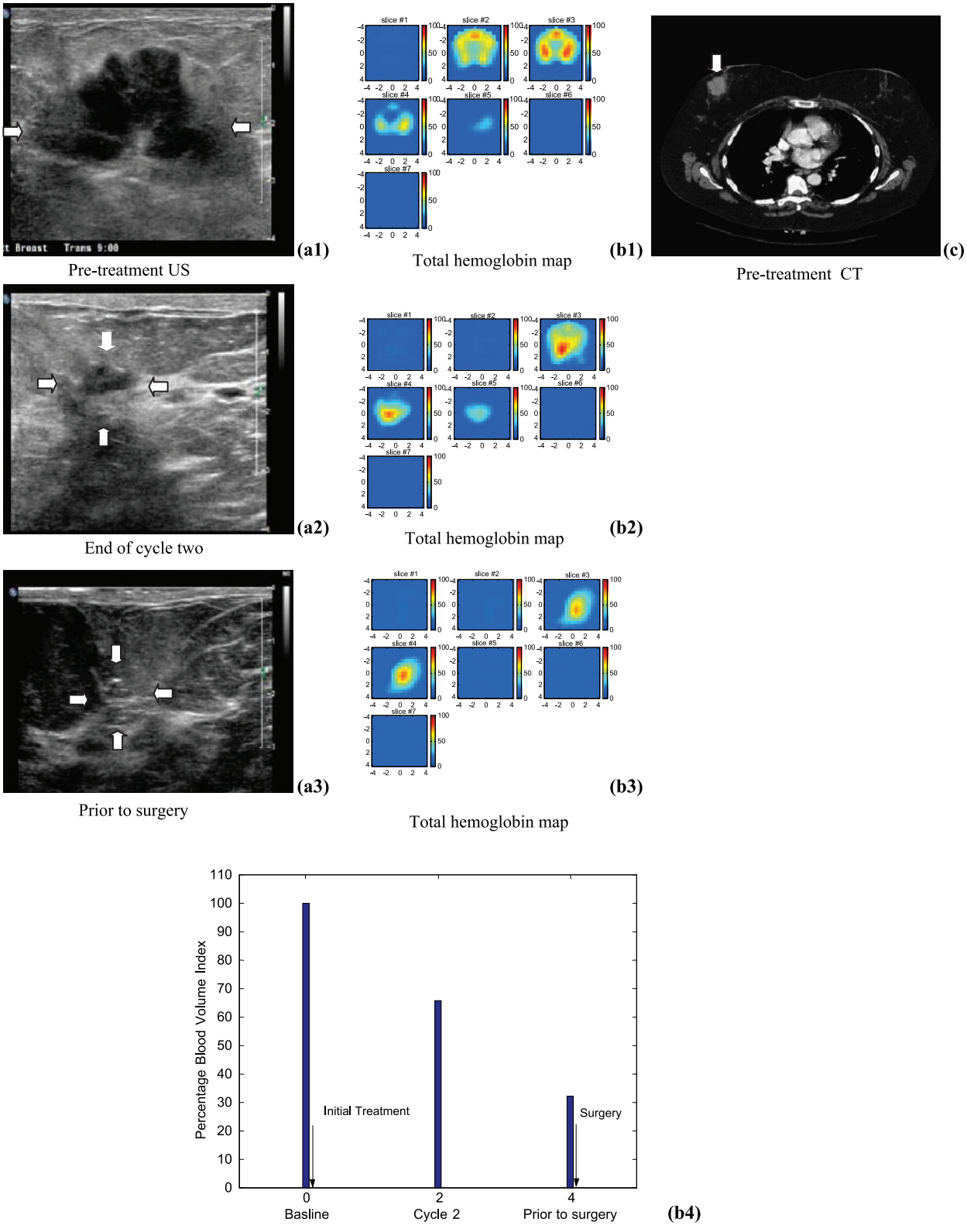

Figure 3. Ultrasound images of a high-grade infiltrating ductal carcinoma (patient 1) obtained before treatment (a1), at the end of cycle two (a2), and before her surgery (a3). US images showed dramatic reduction of tumor size from 4.4 cm to a smaller area visible with the assistance of a metallic marker placed before chemotherapy. (b1) to (b3) are the corresponding tHb maps. In each tHb map, seven slices correspond to spatial images of 9 cm × 9 cm obtained starting at 0.5 cm underneath the skin surface to 3.5 cm deep toward the chest wall with 0.5 cm spacing in depth. The color bar in tHb map is in units of micromoles per liter. The tHb map showed a heterogeneous pattern before treatment and was more confined to a much smaller core area at the end. (c) is a postcontrast CT scan before initial treatment showing a lobulated tumor. (b4) displays the %BVI computed from the NIR hemoglobin images at the three treatment points with the first point measured before treatment as the baseline. The %BVI dropped to 32.1%. This patient received near-complete pathologic response.

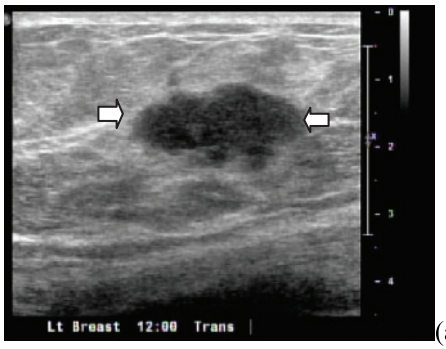

(a1) Pre-treatment US

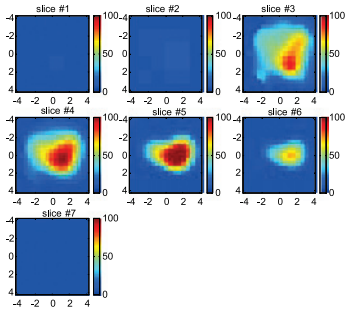

(b1) Total hemoglobin map

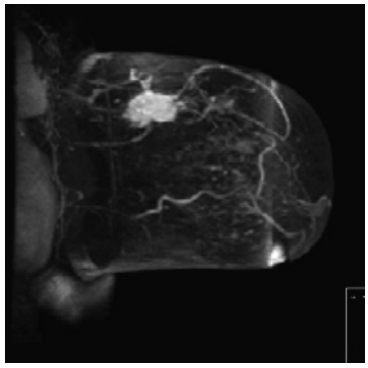

(c1) Contrast Enhanced MRI (pre-chemo)

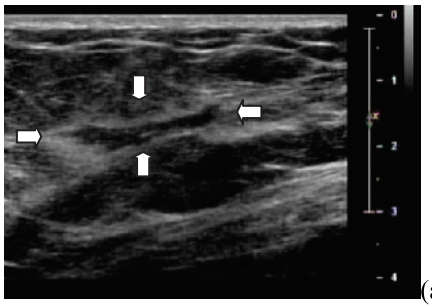

(a2) End of cycle two

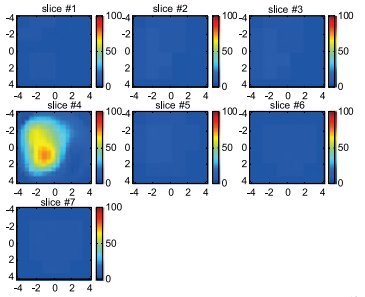

(b2) Total hemoglobin map

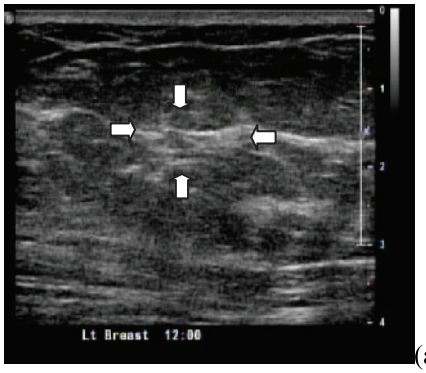

(a3) Prior to surgery

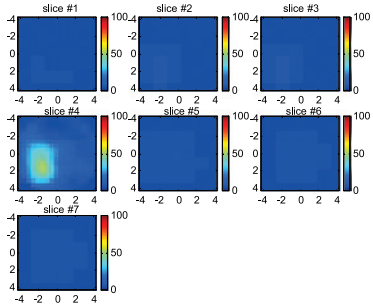

(b3) Total hemoglobin map

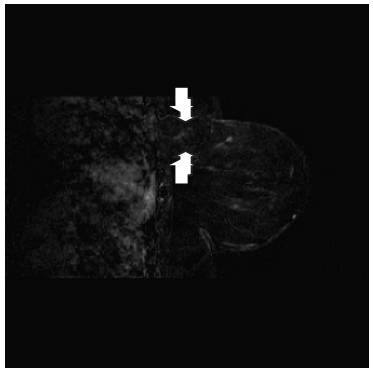

(c2) Contrast enhanced MRI (post-chemo)

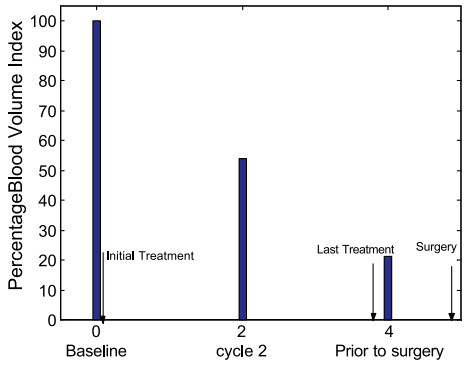

(b4)

Figure 4. US images of a high-grade infiltrating ductal carcinoma (patient 3). (a1) to (a3) are US images acquired the same day before initial treatment, at the end of cycle 2, and before definitive surgery, respectively. US images showed significant reduction in tumor volume at the end of cycle 2. (b1) to (b3) are corresponding tHb concentration maps. In each tHb map, seven slices correspond to a spatial image of 9 cm × 9 cm obtained starting at 0.2 cm underneath the skin surface to 3.2 cm deep toward the chest wall with 0.5 cm spacing in depth. A 62.5 μM/l reduction in hemoglobin level was obtained at the end of the treatment and the corresponding %BVI dropped to 21.1% (b4). (c1) to (c2) are postcontrast subtracted MRI images acquired before initial treatment and before definitive surgery, respectively. MRI image revealed no tumor mass at the end of the treatment. This patient received a complete pathologic response.

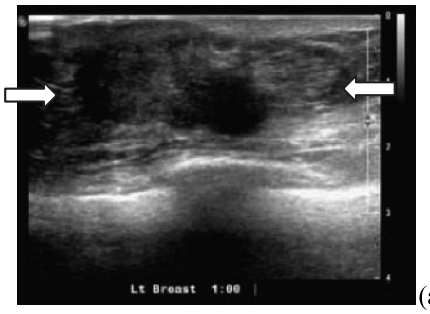

(a1)

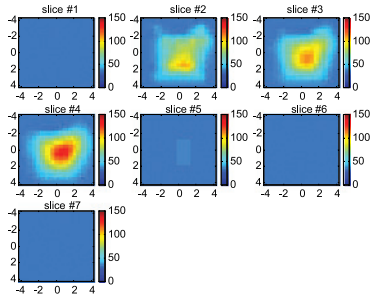

(b1)

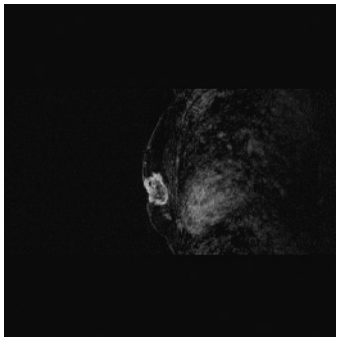

(c1)

Pre-treatment US

Total hemoglobin map

Contrast enhanced MRI (pre-chemo)

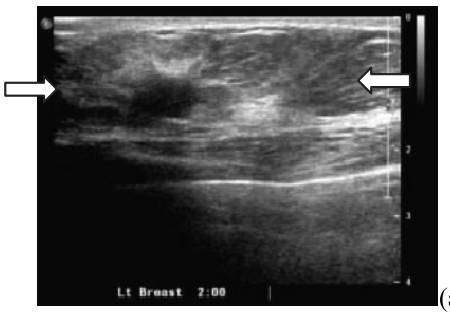

(a2)

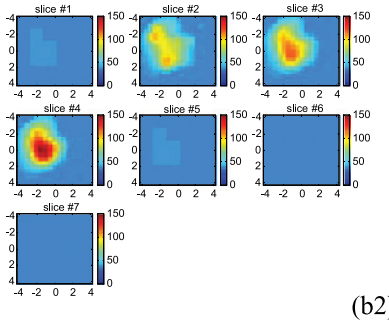

(b2)

End of cycle two

Total hemoglobin map

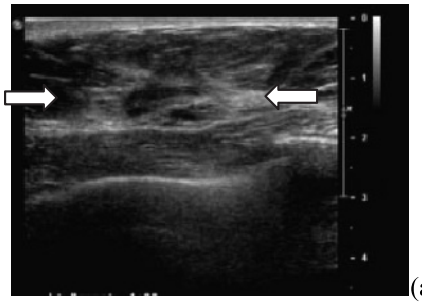

(a3)

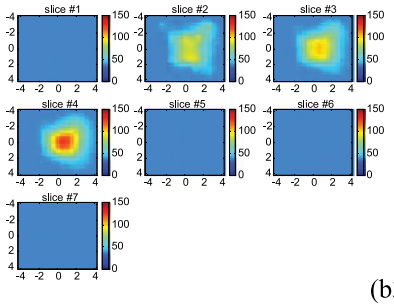

(b3)

End of cycle four

Total hemoglobin map

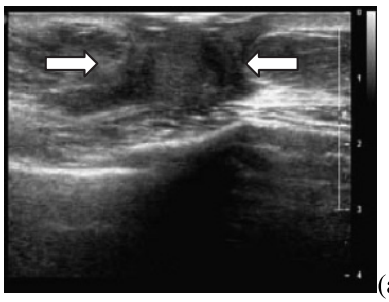

(a4)

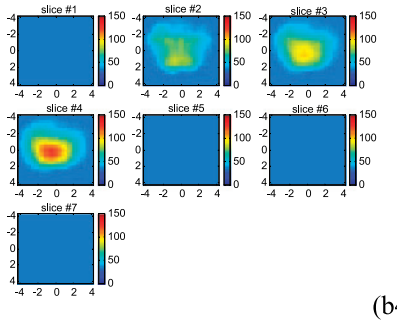

(b4)

End of cycle six

Total hemoglobin map

Figure 5. US images of a low-grade infiltrating ductal carcinoma (patient 11) shown in the left column of (a1) to (a5). The tumor margins shown in the first three US images were not well defined but were better delineated in the last two images (88% reduction from pre- to posttreatment). The middle column of (b1) to (b5) shows corresponding hemoglobin maps from pretreatment (b1) to posttreatment (B5), which reveal substantial blood volume near the chest wall (third slice) throughout the treatment. In each tHb map, seven slices correspond to spatial a image of 9 cm × 9 cm obtained starting at 0.2 cm underneath the skin surface to 3.2 cm deep toward the chest wall with 0.5 cm spacing in depth. (b6) plots the corresponding %BVI from baseline to preoperative assessment every two cycles and no reduction in %BVI was observed. The left column shows postcontrast subtracted MRI images of pretreatment (c1) and posttreatment (c2), respectively. Volume reduction from MRI images is 16%. This patient received a mastectomy and the pathologic residual tumor was 3.3 × 2.8 × 1.2 cm extending to the skin and pectoralis muscle.

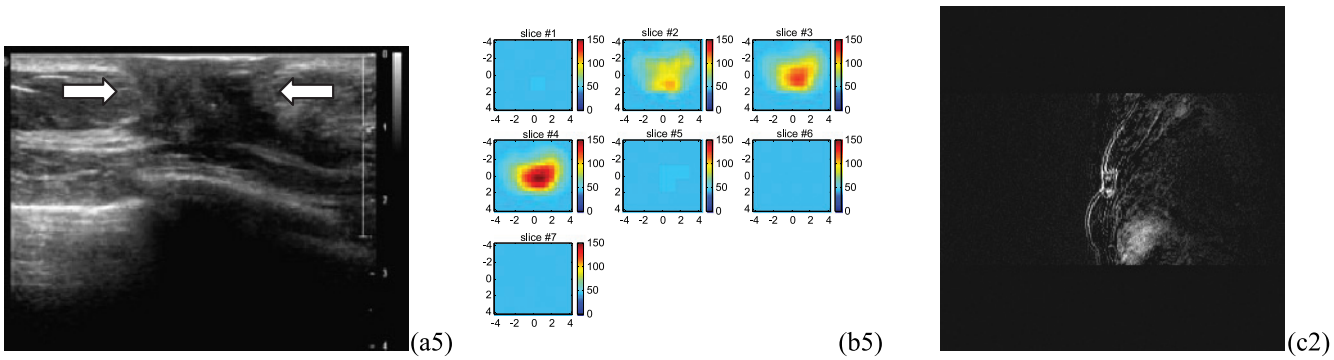

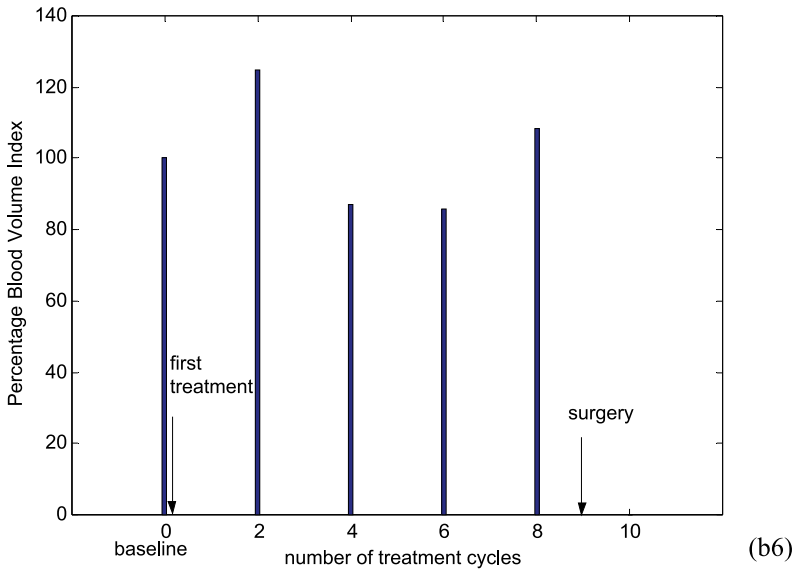

Figure 5. (*continued*)

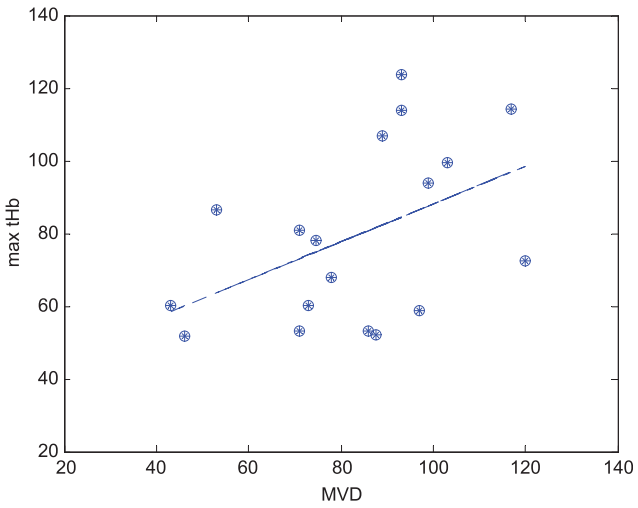

Figure 6. MVD counted from anterior and deep surgical blocks of residual tumor specimens versus tHb maximum values measured at the top and deeper layers in the tHb images. The correlation coefficient of linear regression curve is 0.46, which is moderately significant (P = .0561).

study, Cerussi et al. [34] monitored 11 patients who underwent neoadjuvant chemotherapy before and within 1 week of initial treatment. The authors found that deoxygenated hemoglobin decreased within the first week in pathologically confirmed responders, whereas no significant change was found in nonresponders. In addition, the measured tHb decreased in all responders. In this study, most patients were monitored at pretreatment, cycle 2 and 4, and before surgery. No earlier response data were obtained. However, data of complete and near-complete responder group at cycle 2 do show a noticeable difference in %BVI than partial (B) and nonresponders (C). This suggests that NIR/US may be sensitive enough to identify some responders at earlier treatment cycles. Because our samples are very limited, more patients are needed to validate these initial results.

Another important study objective was to compare vascular response measured by NIR/US with results obtained from conventional US and new imaging modality MRI. In this study, MRI was comparable to NIR/US and was more accurate than US in distinguishing nonresponders from partial responders. MRI, however, is an expensive modality to be used repeatedly during neoadjuvant chemotherapy. In addition, some patients are also troubled by the tight constraints of the MRI machine. However, compared with MRI, optical systems are more cost-effective and portable for use in the

doctors' office, and the flexible light guides can be easily coupled to clinical US probes for repeated imaging. The limitation of our reported comparison study is that only eight patients had MRI imaging results. Nevertheless, the agreement between %BVI results and MRI measurements in accurately classifying the different response groups demonstrates the potential of NIR/US as a cost-effective alternative for monitoring chemotherapeutic response.

Over the last decade, it has become known that hypoxia changes the pattern of gene expression that alters the malignant potential of tumors leading to more aggressive behavior and poor response to various forms of chemotherapy [46,47]. Of the 11 patients, five were imaged with the second prototype featuring an additional wavelength at 690 nm that is more sensitive to deoxygenated hemoglobin changes. We observed a trend that the carcinomas were deoxygenated before the treatment and were more oxygenated toward the end of the treatment. No statistical difference in relative oxygen saturation was observed between responders and nonresponders. Several reports also indicate variable oxygenation changes during chemotherapy [18,27,33], which are in agreement with our preliminary observations. More patient data is needed to obtain statistically valid information on tumor hypoxia changes during chemotherapy. Hypoxia imaging may allow better definition of a population that would benefit from novel anti–hypoxia-directed therapies.

The region of interest (ROI) selection from co-registered US image used for NIR imaging reconstruction should be noted. Optical images were reconstructed by segmenting the volume underneath the probe into a fine-mesh ROI and the background. Because the carcinomas were large in this group of patients, the entire probe size (9×9 cm^2) was used as the ROI in spatial dimensions. Therefore, the reconstructed optical images were independent of tumor spatial dimensions seen by US. In our early phantom study [36], we found no significant difference in reconstructed optical properties when the ROI was twice or three times larger in spatial dimensions than a target 2 to 3 cm in size. The depth localization of NIR diffusive wave is very poor and a tighter ROI in depth dimension is mainly set by co-registered US and therefore depends on margins seen by US. Assisted by chest-wall structure and normal tissue layer structures seen in co-registered US, we can select the ROI in depth dimension reasonably well. In general, we give at least 0.5 cm larger margin in depth than the ultrasonically identified upper and deeper layers. In some difficult cases with unknown margins near the chest wall, we use the chest-wall depth as the deep margin for the ROI.

Optical imaging reconstruction is performed by using the standard perturbation approach where the difference between the measurements obtained at the lesion site and the normal contralateral site is used as the scattered field (U_{sd}) for inversion. Using this approach, we could subtract any changes related to normal breast tissue response to chemotherapy at each monitoring point. Because this approach is sensitive to contralateral site selection, we have checked possible bilateral disease from co-registered US and MRI (if available) and did not find any bilateral disease case in this group of patients. In this study, the two prototype systems used have an identical design in terms of detectors used, source power level at the fiber tips on the probe, and electronic gains. The only differences were the addition of a 690-nm source for better estimation of oxygen saturation and improved system packaging for ease of transportation. Extensive phantom studies have demonstrated comparable performance in target characterization for the two systems. In addition, %BVI is a relative measurement compared to pretreatment baseline for each patient and it is not sensitive to minor system differences as long as the same system is used for each patient.

%BVI is the ratio of measured BVI (product of measured tHb volume and average tHb) at each assessment point over the pretreatment baseline. Errors in tHb estimate can affect the BVI measurements. One type of error is related to the quantification accuracy of tHb. Our phantom studies showed that the estimation accuracy for typical larger absorbers was between 55% and 101% for the typical depth we studied. However, because the %BVI is the ratio of measured BVIs, it is less susceptible to tHb quantification accuracy. Another type of error is related to the repeatability of the tHb quantification at each assessment point. For each patient, we took several data sets at the lesion area and the tHb and the volume reported were average values. The mean variations from the average tHb estimates for this group of patients was 2.3 μM/l, which was 4% of the estimated tHb.

When the NIR/US technique is used to obtain the pretreatment baseline, the data should be taken either before the patient's diagnostic core biopsy or after a certain period. A hematoma after a core biopsy procedure could partially contribute to a higher hemoglobin level, which could be reduced to some extent due to the normal healing process. In our study, baseline data were obtained before the core biopsy in three patients and after in eight patients with an average of 30 days (range, 14 to 52 days). One nonresponder (patient 9) who had her NIR/US study 14 days after core biopsy showed the highest %BVI reduction in this group, which could be partially affected by hematoma. The rest of the seven patients had their NIR/US study at an average of 32 days (range, 20 to 52 days) after initial biopsy.

This pilot study has several limitations, primarily the small population of women with locally advanced cancers. For all patients except one, surgery was performed less than 1 month from posttreatment NIR/US (average, 14 days) and MRI (average, 18 days). One patient (patient 5) had a longer delay between surgery and post-NIR/US (46 days) and MRI (48 days). These intervals were similar to those of other previously reported studies [12,48].

Our initial results have shown that NIR/US using volumetric vascular measurements is a valuable tool in assessing *in vivo* vascular response to neoadjuvant chemotherapy. It is a quick and noninvasive method that may prove invaluable for neoadjuvant treatments to repeatedly monitor the impact of novel agents on vascular distribution. Our initial results support the need to conduct future studies to assess the value of NIR/US in the prediction of early pathologic tumor response and residual disease before surgery.

Acknowledgments

The authors greatly appreciate the assistance of US technologists Kimberly Sokol, Brenda Cameron, Debra Perusse, and Natalie Brown in the Department of Radiology on patient scheduling, US imaging, and patient scanning. The authors greatly appreciate Nancy Baccaro and Ellen Oliver at Neag Cancer Center on patient scheduling.

References

[1] Buchholz TA, Lehman CD, Harris JR, Pockaj BA, Khouri N, Hylton NF, Miller MJ, Whelan T, Pierce LJ, Esserman LJ, et al. (2008). Statement of the science concerning locoregional treatments after preoperative chemotherapy for breast cancer: a National Cancer Institute conference. *J Clin Oncol* **26** (5), 791–797.

[2] Fisher B, Brown A, Mamounas E, Wieand S, Robidoux A, Margolese RG, Cruz AB Jr, Fisher ER, Wickerham DL, Wolmark N, et al. (1997). Effect of preoperative chemotherapy on local-regional disease in women with operable breast

cancer: findings from National Surgical Adjuvant Breast and Bowel Project B-18. *J Clin Oncol* **15** (7), 2483–2493.

[3] Bear HD, Anderson S, Smith RE, Geyer CE Jr, Mamounas EP, Fisher B, Brown AM, Robidoux A, Margolese R, Kahlenberg MS, et al. (2006). Sequential preoperative or postoperative docetaxel added to preoperative doxorubicin plus cyclophosphamide for operable breast cancer: National Surgical Adjuvant Breast and Bowel Project Protocol B-27. *J Clin Oncol* **24** (13), 2019–2027.

[4] Wolmark N, Wang J, Mamounas E, Bryant J, and Fisher B (2001). Preoperative chemotherapy in patients with operable breast cancer: nine-year results from National Surgical Adjuvant Breast and Bowel Project B-18. *J Natl Cancer Inst Monogr* **2001** (30), 96–102.

[5] Sullivan D (2006). Molecular imaging in oncology. *Ann Oncol* **17** (suppl 10), 287–292.

[6] Chagpar AB, Middleton LP, Sahin AA, Dempsey P, Buzdar AU, Mirza AN, Ames FC, Babiera GV, Feig BW, Hunt KK, et al. (2006). Accuracy of physical examination, ultrasonography, and mammography in predicting residual pathologic tumor size in patients treated with neoadjuvant chemotherapy. *Ann Surg* **243** (2), 257–264.

[7] DeMartini W, Lehman C, and Partridge S (2008). Breast MRI for cancer detection and characterization: a review of evidence-based clinical applications. *Acad Radiol* **15** (4), 408–416.

[8] Martincich L, Montemurro F, De Rosa G, Marra V, Ponzone R, Cirillo S, Gatti M, Biglia N, Sarotto I, Sismondi P, et al. (2004). Monitoring response to primary chemotherapy in breast cancer using dynamic contrast-enhanced magnetic resonance imaging. *Breast Cancer Res Treat* **83** (1), 67–76.

[9] Padhani AR, Hayes C, Assersohn L, Powles T, Makris A, Suckling J, Leach MO, and Husband JE (2006). Prediction of clinicopathologic response of breast cancer to primary chemotherapy at contrast-enhanced MR imaging: initial clinical results. *Radiology* **239**, 361–374.

[10] Manton DJ, Chaturvedi A, Hubbard A, Lind MJ, Lowry M, Maraveyas A, Pickles MD, Tozer DJ, and Turnbull LW (2006). Neoadjuvant chemotherapy in breast cancer: early response prediction with quantitative MR imaging and spectroscopy. *Br J Cancer* **94** (3), 427–435.

[11] Weatherall PT, Evans GF, Metzger GJ, Saborrian MH, and Leitch AM (2001). MRI vs. histologic measurement of breast cancer following chemotherapy: comparison with x-ray mammography and palpation. *J Magn Reson Imaging* **13** (6), 868–875.

[12] Delille J-P, Slanetz PJ, Yeh ED, Halpern EF, Kopans DB, and Garrido L (2003). Invasive ductal breast carcinoma response to neoadjuvant chemotherapy: noninvasive monitoring with functional MR imaging—pilot study. *Radiology* **228**, 63–69.

[13] Rousseau C, Devillers A, Sagan C, Ferrer L, Bridji B, Campion L, Ricaud M, Bourbouloux E, Doutriaux I, Clouet M, et al. (2006). Monitoring of early response to neoadjuvant chemotherapy in stage II and III breast cancer by [^{18}F]fluorodeoxyglucose positron emission tomography. *J Clin Oncol* **24** (34), 5366–5372.

[14] Smith IC, Welch AE, Hutcheon AW, Miller ID, Payne S, Chilcott F, Waikar S, Whitaker T, Ah-See AK, Eremin O, et al. (2000). Positron emission tomography using [^{18}F]-fluorodeoxy-D-glucose to predict the pathologic response of breast cancer to primary chemotherapy. *J Clin Oncol* **18** (8), 1676–1688.

[15] Tromberg BJ, Cerussi A, Shah N, Compton M, Durkin A, Hsiang D, Butler J, and Mehta R (2005). Imaging in breast cancer: diffuse optics in breast cancer: detecting tumors in pre-menopausal women and monitoring neoadjuvant chemotherapy. *Breast Cancer Res* **7** (6), 279–285.

[16] Chance B, Nioka S, Zhang J, Conant EF, Hwang E, Briest S, Orel SG, Schnall M, and Czerniecki BJ (2005). Breast cancer detection based on incremental biochemical and physiological properties of breast cancers: a six-year, two-site study. *Acad Radiol* **23**, 925–933.

[17] Poplack SP, Tosteson TD, Wells WA, Pogue BW, Meaney PM, Hartov A, Kogel CA, Soho SK, Gibson JJ, and Paulsen KD (2007). Electromagnetic breast imaging: results of a pilot study in women with abnormal mammograms. *Radiology* **243**, 350–359.

[18] Choe R, Corlu A, Lee K, Durduran T, Konecky SD, Grosicka-Koptyra M, Arridge SR, Czerniecki BJ, Fraker DL, DeMichele A, et al. (2005). Diffuse optical tomography of breast cancer during neoadjuvant chemotherapy: a case study with comparison to MRI. *Med Phys* **32** (4), 1128–1139.

[19] Heffer E, Pera V, Schutz O, Siebold H, and Fantini S (2004). Near-infrared imaging of the human breast: complementing hemoglobin concentration maps with oxygenation images. *J Biomed Opt* **9** (6), 1152–1160.

[20] Gu X, Zhang Q, Bartlett M, Schutz L, Fajardo LL, and Jiang H (2004). Differentiation of cysts from solid tumors in the breast with diffuse optical tomography. *Acad Radiol* **11** (1), 53–60.

[21] Spinelli L, Torricelli A, Pifferi A, Taroni P, Danesini G, and Cubeddu R (2005). Characterization of female breast lesions from multi-wavelength time-resolved optical mammography. *Phys Med Biol* **50** (11), 2489–2502.

[22] Schmitz CH, Klemer DP, Hardin R, Katz MS, Pei Y, Graber HL, Levin MB, Levina RD, Franco NA, Solomon WB, et al. (2005). Design and implementation of dynamic near-infrared optical tomographic imaging instrumentation for simultaneous dual-breast measurements. *Appl Opt* **44** (11), 2140–2153.

[23] Yates T, Hebden JC, Gibson A, Everdell N, Arridge SR, and Douek M (2005). Optical tomography of the breast using a multi-channel time-resolved imager. *Phys Med Biol* **50** (11), 2503–2517.

[24] Athanasiou A, Vanel D, Balleyguier C, Fournier L, Mathieu MC, Delaloge S, and Dromain C (2005). Dynamic optical breast imaging: a new technique to visualise breast vessels: comparison with breast MRI and preliminary results. *Eur J Radiol* **54** (1), 72–79.

[25] Floery D, Helbich TH, Riedl CC, Jaromi S, Weber M, Leodolter S, and Fuchsjaeger MH (2005). Characterization of benign and malignant breast lesions with computed tomographic laser mammography (CTLM). *Invest Radiol* **40**, 328–335.

[26] Brooksby B, Pogue BW, Jiang S, Dehghani H, Srinivasan S, Kogel C, Tosteson TD, Weaver J, Poplack SP, and Paulsen KD (2006). Imaging breast adipose and fibroglandular tissue molecular signatures by using hybrid MRI-guided near-infrared spectral tomography. *Proc Natl Acad Sci USA* **103** (23), 8828–8833.

[27] Shah N, Gibbs J, Wolverton D, Cerussi A, Hylton N, and Tromberg BJ (2005). Combined diffuse optical spectroscopy and contrast-enhanced magnetic resonance imaging for monitoring breast cancer neoadjuvant chemotherapy: a case study. *J Biomed Opt* **10** (5), 051503.

[28] Zhang Q, Brukilacchio TJ, Li A, Stott JJ, Chaves T, Hillman E, Wu T, Chorlton M, Rafferty E, Moore RH, et al. (2005). Coregistered tomographic x-ray and optical breast imaging: initial results. *J Biomed Opt* **10** (2), 024033.

[29] Ntziachristos V, Yodh AG, Schnall MD, and Chance B (2002). MRI-guided diffuse optical spectroscopy of malignant and benign breast lesions. *Neoplasia* **4** (4), 347–354.

[30] Zhu Q, Chen NG, and Kurtzman SH (2003). Imaging tumor angiogenesis by the use of combined near infrared diffusive light and ultrasound. *Opt Lett* **28** (5), 337–339.

[31] Zhu Q, Huang MM, Chen NG, Zarfos K, Jagjivan B, Kane M, Hedge P, and Kurtzman S (2003). Ultrasound-guided optical tomographic imaging of malignant and benign breast lesions. *Neoplasia* **5** (5), 379–388.

[32] Zhu Q, Cronin EB, Currier AA, Vine HS, Huang MM, Chen NG, and Xu C (2005). Benign versus malignant breast masses: optical differentiation with US-guided optical imaging reconstruction. *Radiology* **237**, 57–66.

[33] Zhu Q, Kurtzman S, Hegde P, Tannenbaum S, Kane M, Huang MM, Chen NG, Jagjivan B, and Zarfos K (2005). Utilizing optical tomography with ultrasound localization to image heterogeneous hemoglobin distribution in large breast cancers. *Neoplasia* **7** (3), 263–270.

[34] Cerussi A, Hsiang D, Shah N, Mehta R, Durkin A, Butler J, and Tromberg BJ (2007). Predicting response to breast cancer neoadjuvant chemotherapy using diffuse optical spectroscopy. *Proc Natl Acad Sci USA* **104** (10), 4014–4019.

[35] Chen NG, Guo PY, Yan SK, Piao DQ, and Zhu Q (2001). Simultaneous near infrared diffusive light and ultrasound imaging. *Appl Opt* **40** (34), 6367–6380.

[36] Zhu Q, Xu C, Guo P, Aguirre A, Yuan BY, Huang F, Castilo D, Gamelin J, Tannenbaum S, Kane M, et al. (2006). Optimal probing of optical contrast of breast lesions of different size located at different depths by US localization. *Technol Cancer Res Treat* **5** (4), 365–380.

[37] O'Leary MA, Boas DA, Chance B, and Yodh AG (1995). Experimental images of heterogeneous turbid media by frequency-domain diffusing-photon tomography. *Opt Lett* **20** (5), 426–429.

[38] Therasse P, Arbuck SG, Eisenhauer EA, Wanders J, Kaplan RS, Rubinstein L, Verweij J, Van Glabbeke M, van Oosterom AT, Christian MC, et al. (2000). New guidelines to evaluate the response to treatment in solid tumors. *J Natl Cancer Inst* **92** (3), 205–216.

[39] Sataloff DM, Mason BA, Prestipino AJ, Seinige UL, Lieber CP, and Baloch Z (1995). Pathologic response to induction chemotherapy in locally advanced carcinoma of the breast: a determinant of outcome. *J Am Coll Surg* **180**, 297–306.

[40] Weidner N, Carroll PR, Flax J, Blumenfeld W, and Folkman J (1993). Tumor angiogenesis correlates with metastasis in invasive prostate carcinoma. *Am J Pathol* **143** (2), 401–409.

[41] Makris A, Powles TJ, Kakolyris S, Dowsett M, Ashley SE, and Harris AL (1999). Reduction in angiogenesis after neoadjuvant chemoendocrine therapy in patients with operable breast carcinoma. *Cancer* **85** (9), 1996–2000.

[42] Jakubowski DB, Cerussi AE, Bevilacqua F, Shah N, Hsiang D, Butler J, and Tromberg BJ (2004). Monitoring neoadjuvant chemotherapy in breast cancer using quantitative diffuse optical spectroscopy: a case study. *J Biomed Opt* **9** (1), 230–238.

[43] Perou CM, Sørlie T, Eisen MB, van de Rijn M, Jeffrey SS, Rees CA, Pollack JR, Ross DT, Johnsen H, Akslen LA, et al. (2000). Molecular portraits of human breast tumours. *Nature* **406**, 747–752.

[44] Sørlie T, Perou CM, Tibshirani R, Aas T, Geisler S, Johnsen H, Hastie T, Eisen MB, van de Rijn M, Jeffrey SS, et al. (2001). Gene expression patterns of breast carcinomas distinguish tumor subclasses with clinical implications. *Proc Natl Acad Sci USA* **98** (19), 10869–10874.

[45] Carey LA, Dees EC, Sawyer L, Gatti L, Moore DT, Collichio F, Ollila DW, Sartor CI, Graham ML, and Perou CM (2007). The triple negative paradox: primary tumor chemosensitivity of breast cancer subtypes. *Clin Cancer Res* **13**, 2329–2334.

[46] Hockel M and Vaupel P (2001). Tumor hypoxia: definitions and current clinical, biologic, and molecular aspects. *J Natl Cancer Inst* **93**, 266–276.

[47] Padhani AR (2005). Where are we with imaging oxygenation in human tumours? *Cancer Imaging* **5** (1), 128–130.

[48] Rieber A, Brambs HJ, Gabelmann A, Heilmann V, Kreienberg R, and Kühn T (2002). Breast MRI for monitoring response of primary breast cancer to neoadjuvant chemotherapy. *Eur Radiol* **12** (7), 1711–1719.